Vision Research 230 (2025) 108596

Contents lists available at ScienceDirect

Vision Research

journal homepage: www.elsevier.com/locate/visres

Structural and functional analysis of the eye according to the accommodation-age relationship

María Arcas-Carbonell [a,b], Elvira Orduna-Hospital [a,b,*], Sara Oliete-Lorente [a], María Mechó-García [c], Guisela Fernández-Espinosa [a,b], Ana Sanchez-Cano [a,b]

[a] Department of Applied Physics, University of Zaragoza, 50009 Zaragoza, Spain
[b] Aragon Institute for Health Research (IIS Aragon), 50009 Zaragoza, Spain
[c] Clinical & Experimental Optometry Research Lab, Center of Physics (Optometry), School of Sciences, University of Minho, 4710 - 057 Braga, Portugal

ARTICLE INFO

Keywords:
Aberrometry
Accommodative function
Anterior chamber depth
Retinal curvature
Lens curvature
Age ranges
Optical coherence tomography

ABSTRACT

This study investigates how accommodative demand affects ocular function by examining variations in the anterior chamber depth (ACD), as well as the retinal and anterior surface curvatures of the crystalline lens across different age groups.

The study included 96 right eyes from healthy individuals aged 18 to 66 years. Accommodation was assessed using an aberrometer under demands up to 5 diopters (D). Images of the anterior segment and retina were recorded and analyzed with custom software to adjust these surfaces to conic curves, providing data on changes in ACD, anterior surface curvature of the crystalline lens, and retinal shape during accommodation.

The average age of participants was 35.42 ± 13.55 years. Accommodation matched the demand at low levels (up to 1D) but under-accommodated at higher demands. No significant differences were found in the anterior surface curvature of the crystalline lens with increased accommodation, though a weak trend was observed in younger individuals. ACD significantly decreased with accommodation due to the anterior displacement of the lens. Retinal curvature showed significant changes, including flattening, with increased accommodative demand. There were correlations between the anterior surface eccentricity of the crystalline lens and both ACD changes and retinal eccentricity.

In conclusion, accommodation effectively responds to demands up to 1D across all ages. Our findings suggest a tendency for retinal curvature to flatten to higher demands, requiring further validation. While the central curvature of the anterior surface of the crystalline lens does not change significantly, ACD decreases with accommodation, indicating how age and presbyopia influence accommodative capacity and structural changes in the eye.

1. Introduction

Accommodation in the human visual system is the process by which the crystalline lens changes its power to keep the image of an object in clear focus on the retina, adjusting to its distance. When a person shifts their gaze from far vision (FV) to near vision (NV), morphological changes occur in various structures of the eyeball. These changes lead to an increase in the dioptric power of the lens through the accommodation process, ensuring a sharp image (Atchison & Smith, 2023). This process involves the so-called accommodative triad, which provides an accommodative response followed by miosis and convergence. Therefore, the lens (through the ciliary body and zonules), the pupil (through the sphincter and dilator muscles of the iris), and the extraocular muscles all act together (Kanski & Bowling, 2011). With age, a series of morphological changes occur in the lens: its thickness increases, the nucleus becomes flatter, and the anterior and posterior curvatures change (Giovanzana et al., 2017), additionally, functional variations appear. These changes results in presbyopia, when the near point of the eye is farther than the usual working distance, due to a reduction in the amplitude and speed of accommodation. Presbyopia typically appears around the age of 45, when the amplitude of accommodation (AA) of the lens is approximately 3.5 diopters (D), and more than half of the

* Corresponding author.
E-mail addresses: marcas@unizar.es (M. Arcas-Carbonell), eordunahospital@unizar.es (E. Orduna-Hospital), soliete1@gmail.com (S. Oliete-Lorente), mmechogarcia@fisica.uminho.pt (M. Mechó-García), guiselafernandez@unizar.es (G. Fernández-Espinosa), anaisa@unizar.es (A. Sanchez-Cano).

https://doi.org/10.1016/j.visres.2025.108596
Received 2 August 2024; Received in revised form 30 March 2025; Accepted 30 March 2025
Available online 9 April 2025

accommodative reserve is used for NV. When this happens, the person experiences fatigue and intermittent periods of blurred NV. Besides age, the onset of presbyopia can depend on refractive error, depth of focus, and the subject's activities that require varying levels of clear and sustained NV (Wolffsohn & Davies, 2019).

Traditionally, the study of the anterior segment of the eye can be conducted using corneal topography, a technique that obtains a model of the corneal surface by analyzing the light reflected from Placido's disks projected onto the anterior surface of the cornea, providing precise curvature data of the cornea (Fan et al., 2018). Some topographers also include cameras utilizing the Scheimpflug principle, which allows for capturing tomographic images of the anterior segment of the eye, reaching up to the anterior capsule of the lens. The combination of corneal topography and anterior segment tomography enables the analysis of the corneal morphology across its entire surface, providing elevation and thickness maps, as well as various parameters of the anterior chamber (Mejía-Barbosa & Malacara-Hernández, 2001). This device allows visualization of the anterior capsule of the lens but does not provide any robust parameter that characterizes it, although morphological changes occurring during accommodation can be observed. Koretz et al. found that the curvature of the anterior crystalline lens and the curvature of the anterior boundary of the lens nucleus, changed as a function of accommodation and age (Koretz et al., 2002). Additionally, the same authors observed a similar correlation between the curvature of the anterior and posterior lens surface and age in 100 non-accommodating subjects, but no such correlation was observed for the curvature of boundaries of the lens nucleus (Koretz et al., 2001). The anterior chamber depth (ACD) and volume are crucial for eye health and function, as any alteration in its structure or in the flow of aqueous humor can lead to pathological conditions such as glaucoma (Kanski & Bowling, 2011). In addition, the ACD can undergo natural changes throughout life (Kanellopoulos & Asimellis, 2014) or due to the amount of accommodation necessary to focus images on the retina (Wang et al., 2015).

The retinal shape is crucial for understanding myopia development, with numerous techniques using custom-built or modified instruments to measure peripheral eye length, particularly given the rise in myopia research (Koumbo Mekountchou et al., 2020). The possibility to quantitatively characterize 3D retinal shape by Magnetic Resonance Imaging (MRI) had offered multitude of options (Beenakker et al., 2015). MRI is considered the reference in this type of studies due to the advantage of imaging the whole eyeball. In a small cohort study, Cheng et al. (Cheng et al., 1992) found that all eyes had the same sphero-elliptical shape with independence of the ametropia. However, another analysis (Atchison et al., 2004) described that myopic eyes were elongated. This elongation could occur in different ways, either globally (overall) or specifically along the axis of the eye. Previous studies have identified changes in retinal curvature associated with myopia development (Ishii et al., 2011; Li & Fang, 2021; Verkicharla et al., 2012) and aging (Faria-Ribeiro et al., 2014), suggesting that retinal shape is not fixed but can adapt depending on ocular conditions and refractive states. Eye models have previously been developed describing the retinal curvature as an ellipsoid incorporating both decentration and orientation, such models indicate that retinal shape deviates from an ellipsoid as the eye becomes more myopic (Li and Fang, 2021). This study found that both myopic and emmetropic eye models have oblate retinas, while the oblateness is lower for the myopes, with similar patterns described by other assessed data (Atchison et al., 2005; Pope et al., 2017; Verkicharla et al., 2016, 2017). Ishii et al. (Ishii et al., 2011) saw that myopia development in children is associated with a transition from oblate to prolate eyeball shape but eye shape and retinal shape are not the same; an eye shape may be described as prolate because the length is longer than the width and/or height, but the corresponding retinal shape might be oblate. It appears that merely categorizing an eye shape as prolate or oblate is inadequate without understanding the contributing parameters. In myopia, a prolate eye shape is likely characterized by a steepening of the retina near the posterior pole and a flattening as it extends away from the pole (Verkicharla et al., 2012). Even, in absence of accommodation, differences in shape from nasal to temporal areas were described and steeper retinas were predicted in older subjects (Faria-Ribeiro et al., 2014). So, retinal shape could also contribute to elucidate the behavior of the eye under the myopia forced during the accommodation process, being the interest in our study to elucidate changes in shape related to the accommodation and NV tasks when other differences such as the retinal thickness can be found (Fan et al., 2014; Orduna-Hospital et al., 2022).

The main objective of this work is to examine the accommodative function and morphological variations in the anterior and posterior ocular structures as accommodative demand increases across a sample of healthy people and in different age groups. Increased accommodative demand results in significant optical and morphological changes in these eye structures, that could be observable and quantifiable in the images provided by these devices. These changes could reflect the visual system's adaptations to the varying visual demands associated with aging and accommodation capacity.

2. Material and methods

2.1. Sample description and measurement performance

The study adhered to the Declaration of Helsinki and was approved by the Clinical Research Ethics Committee of Aragón (CEICA) (approval number 23/479). It included 96 healthy participants, aged 18 to 66 years, each contributing one right eye (RE). Of these, 38 were men and 58 were women. All participants provided informed consent. Inclusion criteria were age 18–69, no binocular or accommodative problems, corrected visual acuity > 0.8 in the RE, refractive error $<$ -4.50D for myopia, $< +2.50$D for hyperopia, and < 1.50D for astigmatism. Participants needed to be free of ocular or systemic diseases affecting vision and have axial length (AL) of 22–26 mm, ensuring that observed retinal changes were solely due to accommodative effort, not axial elongation. Additionally, the study subjects were divided into five age groups: G1 from 18 to 29 years ($n = 48$), G2 from 30 to 39 years ($n = 18$), G3 from 40 to 49 years ($n = 10$), G4 from 50 to 59 years ($n = 12$), and G5 aged 60 years and older ($n = 8$). They attended sessions without contact lenses and abstained from caffeine, alcohol, tobacco, or stimulants for 2 h before measurements.

AA (measured in D) was assessed for each subject using Donders' push-up method, taking the average of three measurements. Monocular accommodative facility (MAF) was evaluated at 40 cm using a $\pm$ 2D flipper, with results recorded in cycles per minute (cpm). AL measurements were obtained using the IOL Master 500 optical biometer (Carl Zeiss Meditec, Oberkochen, Germany). The spherical equivalent (SE) of the participants was measured using the IRX3 Shack-Hartmann aberrometer (Imagine Eyes, Orsay, France). Eight retinal scans (four central and four peripheral) were performed with the 3D OCT-1000 (Topcon Corporation, Tokyo, Japan) while stimulating the subjects' accommodation. For the central retina evaluation, the subject was instructed to fixate on the internal central fixation stimulus of the OCT device, capturing images within the central 30° of the retina. Peripheral retina measurements were obtained by shifting the internal fixation stimulus 15° horizontally toward the temporal area (to the subject's right). This allowed the acquisition of temporal peripheral retina images. This process started with the lens that corrected each subject's SE, followed by the addition of lenses calculated to stimulate 1, 3, and 5D of accommodation. These lenses were placed on a support near the eye. Additionally, four scans with the Galilei G2 Dual Scheimpflug Analyzer (Ziemer Ophthalmic Systems AG, Port, Switzerland) were conducted to study the anterior segment of the subjects. Accommodation was stimulated using the device's integrated automatic mode, which guided the subjects through accommodative demands of 0, 1, 3, and 5D.

2.2. Posterior and anterior pole data

The TopcomExtract 1.0 program (University of Zaragoza, Zaragoza, Spain) was custom-built and used to export central and peripheral retinal images obtained with OCT by directly processing raw FDA format files without modifications (Orduna-Hospital et al., 2024). While these raw images maintain the curvature as captured by the OCT device, they are subject to axial scaling effects due to the refractive index. However, since our study focuses on transversal rather than axial measurements, any potential impact on retinal curvature would be limited. So, retinal curvature measurements were obtained from uncorrected OCT scans to ensure consistency across imaging conditions. A preliminary validation with curved lenses (1.5 refractive index), a parallel-sided lens of 0D, and negative lenses (−1 to −8D) confirmed that optical changes did not distort the center of the raw images, supporting the reliability of this approach for assessing intra-subject relative changes (Supplementary material). For each subject in the study, images of both central and peripheral retina were obtained at baseline (0D accommodation) and at the accommodation stimulus levels of 1, 3, and 5D.

From each FDA file, 128 images in PNG format were extracted, corresponding to the 128 retinal B-scans obtained from the OCT's 6 × 6 mm macular cube protocol, covering 30° of the explored retina, FDA files (Topcon's proprietary format) containing processed 3D OCT 1000 image data and metadata from each subject to extract retinal images. Among these 128 images, the one with the foveal reflex was selected as the central image and thus served as the reference point for selecting the two superior and two inferior ones. Consequently, the 5 central images of the retina were chosen. This process was repeated with the 8 FDAs from each subject, thereby obtaining 5 images of the central and the peripheral retina at baseline and at the three accommodative demands.

For the analysis of the five images per measurement exported using the TopcomExtract 1.0 program, other software, ImgOCT 1.12 (University of Zaragoza, Zaragoza, Spain), was created. Within this program, Image 1 of 5 was selected corresponding to an image of the peripheral retina (on the left), and Image 1 of 5 corresponding to the central retina (on the right) of the RE of the same subject and for the same accommodative demand. Once positioned, 5 matching points from each image were selected, and the program combined the central and peripheral retinas (Fig. 1A). This process was repeated to merge the 5 peripheral images with the 5 central images, resulting in 5 retinal sections of 9 mm in length. Each resulting image was processed in another section of the program, where 5 points from the retinal profile, corresponding to the retinal pigment epithelium (RPE), were selected so that the program could calculate the fitting conic (Fig. 1B). In this step, the retinal curvature descriptor parameters corresponding to the conical adjustment described in the next point were obtained, such as eccentricity, asphericity and shape factor (e, Q, and SF, respectively). These data from the 5 sections per measurement were automatically saved in a text file and subsequently recorded in an Excel database (Microsoft® Office Excel 365, Microsoft Corporation, Redmond, WA, USA).

The Galilei G2 device generated ZIP compressed folders containing raw files for each measurement with each accommodative demand (4 per eye). These folders were extracted and processed using a custom-built software, GalileiConverter 1.0 (University of Zaragoza, Zaragoza, Spain), to automatically obtain and preserve the folder hierarchy, the 16 axial images of the anterior pole in PNG format, which the Galilei G2 captures for each measurement. This process ensured that the images were not automatically processed by the device's built-in software,

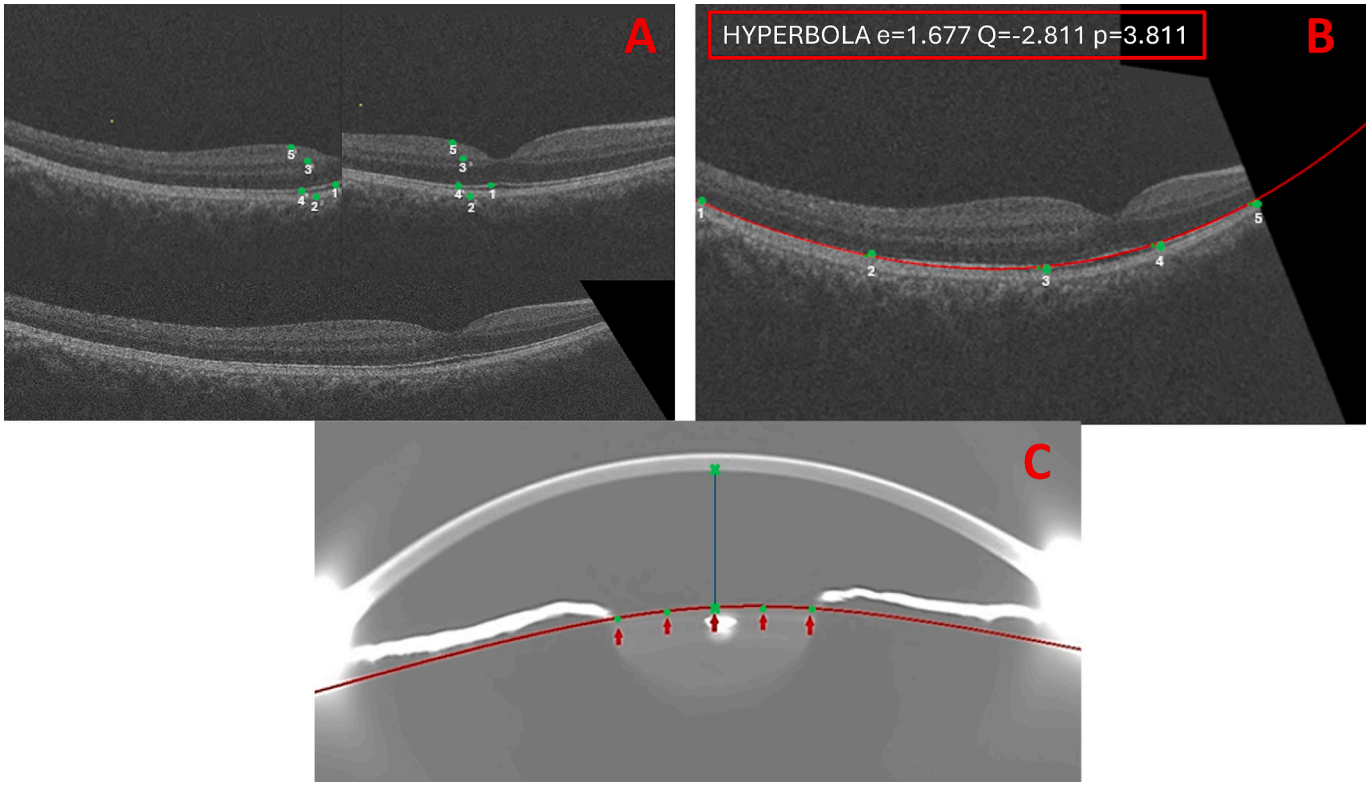

Fig. 1. A) Posterior pole analysis. Program with the 5 selected points on the peripheral retina image (left) and on the central retina image (right) and below the result of combining the central and peripheral retina images. **B)** Posterior pole analysis. Program in the process of selecting the 5 points from the retinal pigment epithelium (RPE) for the subsequent fitting conic calculation on the combined image of the peripheral and central retina. The areas marked with red squares indicate the conic parameters characterizing retinal curvature. **C)** Anterior pole analysis. Program window showing brightness and contrast settings belonging to the first Scheimpflug camera. The 5 points marked on the anterior lens capsule for the calculation of the conical fit parameters are highlighted in green and with a red arrow. The green crosses correspond to points 6 and 7 (connected by the blue line) used to measure the ACD. (For interpretation of the references to colour in this figure legend, the reader is referred to the web version of this article.)

preventing any modifications to the original data. Only image number 1 from the first Scheimpflug camera was selected (Fig. 1C). The tomographic image of the anterior pole was imported into the ImgOCT 1.12 software, and the contrast and brightness were adjusted to 2 and 100, respectively (Fig. 1C). Additionally, 5 points were established on the anterior capsule of the lens to obtain the conical adjustment parameters to evaluate changes in the anterior curvature of the lens with different accommodative demands (Fig. 1C). Points 6 and 7 were also established at the corneal apex and the lens reflex, respectively, to measure the ACD, considering that the AL of each pixel equated to 28 μm. This equivalence was determined by comparing the known corneal thickness in microns (pachymetry) at the apex with the corresponding pixel count in images, allowing for accurate calibration. The data were then automatically exported to a text document and transferred to an Excel database containing lens curvature and ACD data for all subjects across all accommodative demands (0, 1, 3, and 5D).

By using these custom-designed software tools, we ensured that the measurements of both retinal and lens curvatures were obtained with minimal alteration, providing more reliable results than traditional methods that rely on enhanced images or generic corrections.

2.3. Calculation of eccentricity, asphericity and shape factor

The calculation of (e, Q, SF) for both retinal and lens curvature was based on fitting the curve according to the general conic equation (Eq. (1)):

$$ax^2 + 2hxy + by^2 + 2gx + 2fy + n = 0 \quad (1)$$

The intersection of a plane with a cone, when it is not passing through the vertex, results in four distinct types of curves: hyperbola, parabola, ellipse, and circle (Ahn et al., 2001; Rutter, 2018). As the eccentricity value of an ellipse approaches 1, the shape of the conic section gradually flattens. When $e = 1$, the resulting figure becomes a parabola and with $e = 0$, a perfect circle is obtained. Therefore, eccentricity increases, the ellipse tends to flatten. When $e > 1$, the conic section becomes a hyperbola (Downs, 2003).

The data for each subject measured in the image by the ImgOCT 1.12 program are governed by a series of coordinates that vary based on the arrangement of each point. These coordinates are used to calculate the parameter e, (Eq. (2)):

$$e^2 = 2\sqrt{(a-b)^2 + 4h^2}/(\sigma(a+b) + \sqrt{(a-b)^2 + 4h^2}) \quad (2)$$

To determine the sign (σ) of the e, the program uses the following formula (Eq. (3)):

$$\sigma = sign(nh^2 - abn + af^2 - 2hfg + bg^2) \quad (3)$$

The Q value describes the degree of variation in curvature of a surface from its center to its periphery (Eq. (4)). A $Q = 0$ indicates a spherical surface, with no difference between the central and peripheral radii. If $Q < 0$, it signifies a prolate profile with progressive flattening towards the periphery, meaning the center is more curved than the periphery. Conversely, if $Q > 0$, it denotes an oblate profile, where the periphery has greater curvature than the center of the surface (Calossi, 2007; Ying et al., 2012).

$$Q = -e^2 \quad (4)$$

Finally, the SF combines (e, Q) to characterize the precise shape of the surface (Eq. (5)):

$$SF = 1 - Q \quad (5)$$

These parameters used to assess the curvature of the lens and retina are dimensionless, without measurement units. In this work, these parameters are applied to examine the changes occurring in the surface of the anterior lens capsule and the retina as the accommodative demand increases.

2.4. Statistical analysis

All data collected throughout this study were exported to Excel databases for the creation of graphical figures and subsequent statistical analysis using the Statistical Package for the Social Sciences (SPSS 24.0 Inc., Chicago, IL, USA).

Descriptive statistics were performed on the sample according to quantitative variables, calculating the mean, standard deviation (SD), maximum, and minimum for each. The normality of the variables was also assessed with the Kolmogorov-Smirnov test, which indicated that the variables did not follow a normal distribution. Non-parametric tests for related samples (Friedman test) were used to examine whether there were differences between the conical parameters by comparing the four levels of induced accommodation (0, 1, 3, and 5D). Bonferroni correction was applied for six possible pairwise comparisons, with a significance level set at $p < 0.0083$ considered statistically significant. The same procedure was followed by analyzing curvature parameters of the retina, the anterior surface of the lens, and ACD, both for the entire sample and when divided into subgroups.

The Kruskal-Wallis test for k independent samples was used to compare ACD across the five groups, and Bonferroni correction was applied for the ten possible pairwise comparisons, considering a significance level of $p < 0.005$ statistically significant. To correlate parameters of the anterior and posterior poles, the bivariate correlation test with Spearman's rho was used, with a significance level of $p < 0.05$ considered statistically significant.

3. Results

RE from 96 health subjects participated in this study, of which 38 were men (39.58 %) and 58 were women (60.42 %), with a mean age of 35.42 ± 13.55 years (range 18 to 66 years). Participants had a mean AL of 23.98 ± 0.91 mm. The mean ACD of the participants was 3.47 ± 0.37 mm. The mean SE was −2.08 ± 1.72D. (Table 1, Total Group (TG)).

3.1. Analysis of visual function: accommodation

According to the visual function of the TG of subjects, the AA had a mean of 5.88 ± 5.61D and the MAF of the participants, measured in cpm, was 6.06 ± 6.85 cpm (Table 1, TG). Additionally, Table 1 shows that when dividing the sample by age groups, both AA and MAF decrease with aging. The real accommodative ability of the study subjects was also assessed as a visual function parameter while demanding different accommodative demands, ranging from 0 to 5D (Fig. 2).

Fig. 2 shows the average accommodation, objectively measured with the aberrometer, obtained by considering the total sample of subjects. It was found that when no accommodation was required (0D), the subjects started with approximately 0.50D of additional accommodation. At 1D of accommodation demand, the required and the actually achieved accommodation by the subjects matched. As the accommodative demand increased, it was observed that subjects accommodated less than required on average.

3.2. Analysis of the posterior pole: retinal curvature

The retinal curvatures were collected and compared considering the study parameters, including (e, Q, SF), for the four previously described measurements: baseline (0D) and after stimulating accommodation with lenses of −1D, −3D, and −5D, for all eyes of the evaluated subjects.

Statistically significant differences were detected using the Friedman test in the TG ($\chi^2(3) = 112.88$, $p < 0.001$), along with a trend of increase (in absolute value) in the three analyzed parameters as the required accommodative demand increased. Post-hoc pairwise comparisons revealed significant changes between all levels ($p < 0.0083$), indicating a progressive retinal flattening. Fig. 3A shows a positive increase in (e, SF), and a negative change in Q. To enhance the observation of the

Table 1
Characteristics of the sample regarding the number of subjects (n), gender with the number of males and females (M/F), mean ± standard deviation axial length (AL), anterior chamber depth (ACD), spherical equivalent (SE), amplitude of accommodation (AA), and monocular accommodative facility (MAF) of the right eye, considering the sample as a whole (TG) and by age groups.

	n	Age (years)	Gender (M/F)	AL (mm)	ACD (mm)	SE (D)	AA (D)	MAF (cpm)
TG	96	35.42 ± 13.55	38/58	23.98 ± 0.91	3.47 ± 0.37	−2.08 ± 1.72	5.88 ± 5.61	6.06 ± 6.85
G1	48	24.58 ± 2.15	14/34	23.87 ± 0.90	3.61 ± 0.30	−1.96 ± 1.40	10.39 ± 3.27	11.71 ± 4.61
G2	18	34.00 ± 3.32	10/8	24.35 ± 0.39	3.63 ± 0.21	−3.50 ± 1.23	9.31 ± 5.86	7.10 ± 7.78
G3	10	46.00 ± 3.24	6/4	24.79 ± 1.06	3.43 ± 0.34	−2.80 ± 1.89	1.63 ± 2.59	1.56 ± 4.22
G4	12	54.67 ± 3.01	8/4	23.82 ± 1.06	3.20 ± 0.23	−1.04 ± 2.35	0.73 ± 0.99	0 ± 0
G5	8	61.50 ± 1.00	6/2	23.04 ± 0.55	2.77 ± 0.09	−0.31 ± 0.38	0.47 ± 1.00	0 ± 0

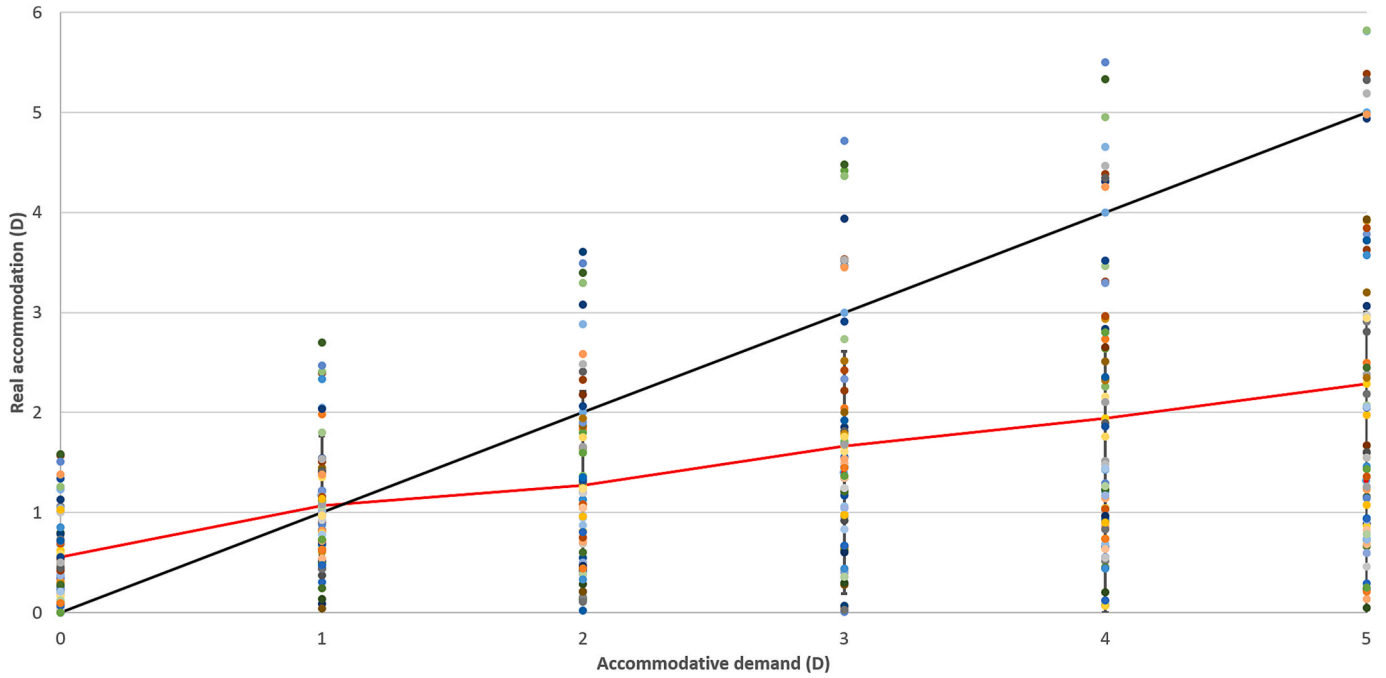

Fig. 2. Visual function mean results of the total group (TG) obtained with the aberrometer, showing the actual accommodation performed at the five levels of accommodative demand, both measured in diopters (D). The black line represents the theoretical amplitude of accommodation (AA) at each accommodative demand level. The red line shows the mean actual accommodation considering the TG at each required accommodation. The vertical lines represent the standard deviation (SD) of the means at each accommodation level, and the colored points represent the actual accommodation performed by each study subject. (For interpretation of the references to colour in this figure legend, the reader is referred to the web version of this article.)

results, changes in the three parameters were assessed relative to the baseline value settled as the unit, and each accommodative state was compared to this reference (Fig. 3B). It can be observed that there is a significant increase in all three studied parameters as the accommodative demand rises up to 5D.

After dividing the sample into the five previously defined age groups. Statistically significant differences with Friedman test were found in groups G1: $\chi^2(3) = 54.81$, G2: $\chi^2(3) = 24.71$ and G3: $\chi^2(3) = 21.44$, all with $p < 0.001$ and across all three curvature parameters (Fig. 3C, D, E), with an absolute increase in their values as the accommodative demand increased, resulting in the retina flattening with increased accommodation. Although there are changes in the evaluated parameters in groups G4 ($\chi^2(3) = 9.00$, $p = 0.029$)and G5 ($\chi^2(3) = 9.00$, $p = 0.029$), these are not statistically significant (both with $p > 0.0083$) as these subjects are presbyopic, having diminished accommodative capacity (Fig. 3F, G). During the tests, these subjects were required to accommodate to a degree that they had reduced or lost, resulting in retinal changes, but to a lesser extent.

A significant negative correlation was observed between AL and SE both in the total group (TG; $r = -0.699$; $p < 0.001$) and in four of the five age groups: G1 ($r = -0.671$; $p < 0.001$), G2 ($r = -0.769$; $p = 0.003$), G4 ($r = -0.799$; $p = 0.006$), and G5 ($r = -0.326$; $p = 0.008$), except for G3 ($r = -0.153$; $p = 0.634$). Correlations between SE and retinal eccentricity were analyzed for the TG and the younger groups (G1 and G2). Significant differences in retinal eccentricity were observed at baseline (0D) and during accommodation (3D), highlighting the relationship between refractive error and retinal shape parameters in these groups. Specifically, in the TG, statistically significant differences were observed both in 0 and 3D of accommodation ($r = -0.233$; $p = 0.028$ and $r = -0.215$; $p = 0.042$, respectively) (Fig. 4A). According to the young groups, in the case of G1 the statistically significant differences were observed in the 3D of accommodation ($r = -0.319$; $p = 0.024$) (Fig. 4B) and in the G2, in the 0D of accommodation ($r = -0.709$; $p = 0.010$) (Fig. 4C).

3.3. *Anterior pole analysis: anterior surface curvature of the crystalline lens*

When analyzing the results of anterior surface of the crystalline lens curvature across the TG, no statistically significant differences with Friedman test ($\chi^2(3) = 1.98$, $p = 0.577$) were found in any of the cases examined with increased accommodation. However, a trend towards increased curvature is observed, with a slight decrease in eccentricity with 5D during the accommodative process (Fig. 5A). As the results were not statistically significant, no post hoc comparisons were made.

Fig. 3. A) Mean results of the studied parameters for the posterior pole, including eccentricity, asphericity, and shape factor of the retina from the total group (TG), both at baseline and after being stimulated with three levels of accommodation using lenses of −1D, −3D, and −5D. Statistically significant differences ($p < 0.0083$), determined by the Friedman test, are indicated with an asterisk (*). **B)** Mean relative results of the studied parameters of the posterior pole: eccentricity, asphericity, and shape factor of the retina in the TG. Results of the baseline measurement, taken as a reference with a value of 1, are shown, along with the stimulation under three accommodation demands using −1D, −3D, and −5D lenses. **C, D, E, F, G)** Mean results of the studied parameters of the posterior pole, including eccentricity, asphericity, and shape factor of the retina, separating the subjects into five age groups (G1, G2, G3, G4 and G5, respectively), in the baseline state, and when stimulated with the three accommodation demands using −1D, −3D, and −5D lenses. Statistically significant differences ($p < 0.0083$), calculated using the Friedman test, are marked with an asterisk (*). In A, C, D, E, F and G, standard deviations are represented with error bars for each case. In all cases, the parameters of eccentricity, asphericity, and shape factor are dimensionless and, therefore, do not have units.

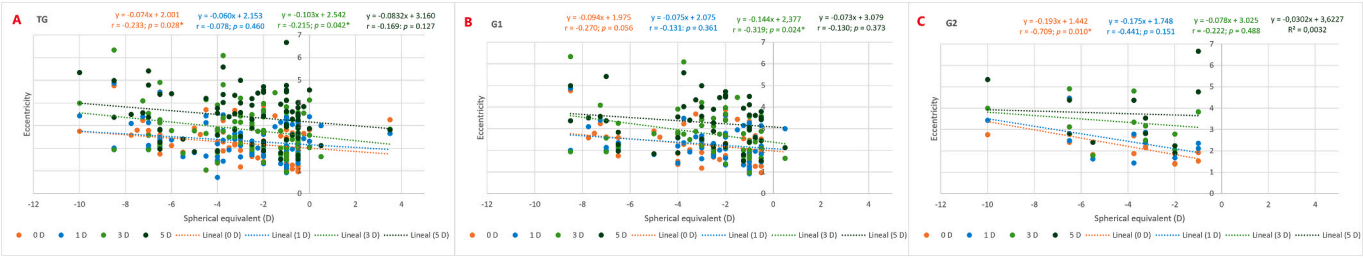

Fig. 4. Correlation analysis between spherical equivalent (SE) and retinal eccentricity for the total group (TG) **(A)** and the younger groups (G1 and G2) **(B** and **C)**. Regression lines for the correlations of eccentricity with SE are displayed, along with the corresponding equations for each line, the correlation coefficient (r), and statistical significance for the 0, 1, 3 and 5D of accommodation. Statistical significance was set at $p < 0.05$ and is marked with an asterisk (*).

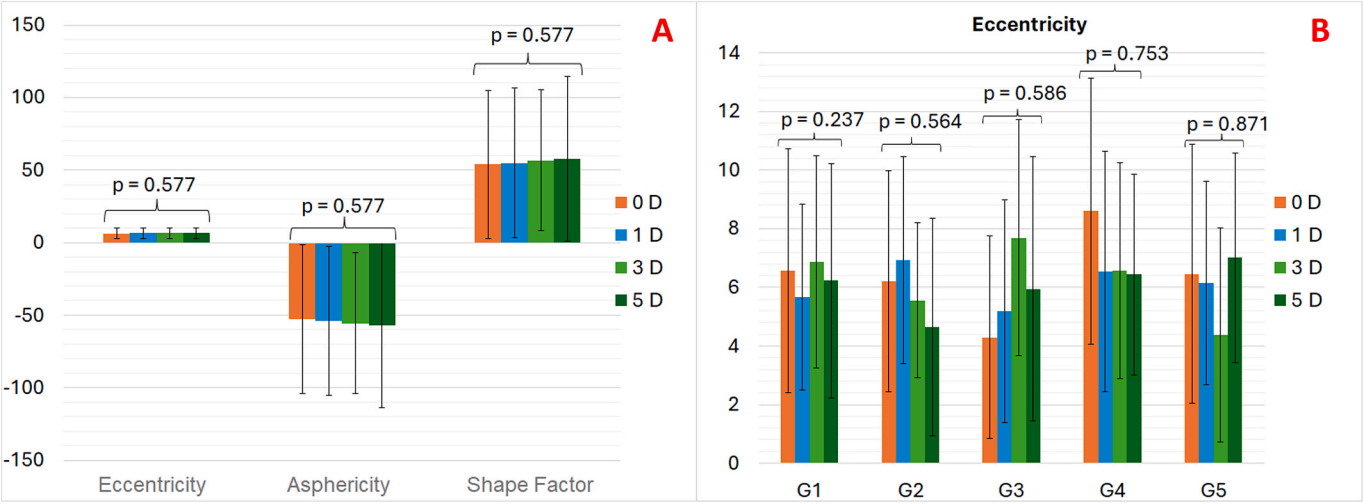

Fig. 5. **A)** Mean results of the parameters of eccentricity, asphericity, and shape factor of the anterior capsule curvature of the lens, considering the TG. Results are shown for the baseline measurement and under accommodation stimulation with −1D, −3D, and −5D lenses. No statistically significant differences ($p > 0.0083$) were found, as calculated using the Friedman test. **B)** Mean results of the eccentricity parameter of the anterior capsule curvature of the lens, separated by the five age groups, for the baseline measurement and under accommodation stimulation with −1D, −3D, and −5D lenses. No statistically significant differences ($p > 0.0083$) were found, as calculated using the Friedman test. Standard deviations are represented with error bars for each case. In all cases of the figure, the parameters of eccentricity, asphericity, and shape factor of the anterior capsule curvature are dimensionless and, therefore, do not have units.

Analyzing lens curvature by age groups, no statistically significant differences were observed with increasing accommodation. The Friedman test results for the groups were as follows: G1 ($\chi^2(3) = 4.23$, $p = 0.237$), G2 ($\chi^2(3) = 2.04$, $p = 0.564$), G3 ($\chi^2(3) = 1.93$, $p = 0.586$), G4 ($\chi^2(3) = 1.20$, $p = 0.753$) and G5 ($\chi^2(3) = 0.71$, $p = 0.871$). However, a trend was noted where, with increasing accommodative demand, particularly with 5D, e value decreased in groups G1, G2, and G3, and even slightly in G4, indicating greater lens curvature (Fig. 5B). In contrast, in G5, the high presbyopic group, attempts to accommodate such power ceased as they were unable to do so, resulting in anterior

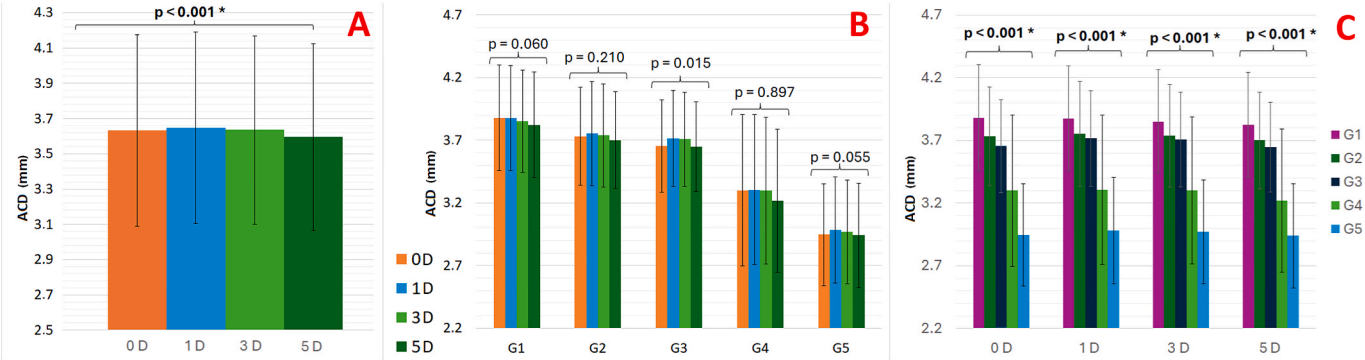

Fig. 6. **A)** Anterior chamber depth (ACD) mean results in the total group (TG), measured in mm, at baseline and during accommodation stimulation with −1D, −3D, and −5D lenses. Statistically significant differences ($p < 0.0083$), calculated using the Friedman test with Bonferroni correction, are marked with an asterisk (*). **B)** ACD mean results in each age group for baseline measurements and during accommodation stimulation with −1D, −3D, and −5D lenses. No statistically significant differences ($p > 0.0083$) were found, calculated using the Friedman test with Bonferroni correction. **C)** ACD mean results for baseline measurements and under accommodation stimulation with −1D, −3D, and −5D lenses in different age groups. Statistically significant differences ($p < 0.005$), as calculated using the Friedman test with Bonferroni correction, are marked with an asterisk (*). Standard deviations are represented with error bars for each case.

surface lens flattening. Equivalent behavior was observed in the parameters (Q, SF), not shown. As no significant differences were found, no post hoc comparisons were made.

3.4. Anterior pole analysis: anterior chamber depth

Fig. 6A shows the changes in the ACD with increased accommodation in the TG. It is observed that the ACD decreases significantly (Friedman test: $p < 0.001$, post-hoc pairwise comparisons with Bonferroni correction revealed significant changes with $p < 0.0083$) as accommodation increases, due to the progressive forward displacement of the lens. In the analysis by age groups, it is observed that the ACD decreases in all groups as accommodation is induced, although no statistically significant changes were found ($p > 0.0083$) (Fig. 6B). However, it is noted that ACD is significantly narrower in older age groups across all accommodation levels ($p < 0.001$), with the narrowest ACD observed in G5 (Fig. 6C). The Kruskal-Wallis test with Bonferroni correction ($p < 0.005$) was applied for pairwise comparisons between groups. This could be related to the lower myopia suffered by these subjects together with the possible increased lens thickness associated with aging.

A weak but significant positive correlation was observed between ACD thickness and anterior surface of the lens eccentricity value during 3D accommodation (with a Spearman's rho correlation coefficient of $r = 0.201$; $p = 0.011$). This indicates that as ACD decreases during 3D accommodation, the anterior lens capsule also decreases in eccentricity value by becoming more curved. A significant negative correlation (with a Spearman's rho correlation coefficient of $r = -0.254$; $p = 0.041$) was found between the eccentricity values of the anterior surface of the lens and the retina during 1D accommodation. As lens eccentricity decreases, retinal eccentricity increases, indicating that as the lens curves to accommodate 1D, a flattening of the retina is observed.

4. Discussion

Recent advancements in measuring accommodation accuracy now incorporate total ocular aberrations and objective methods like double-pass techniques (Aldaba et al., 2012). In this study we used an aberrometer to objectively measure accommodation from 0 to 5D. At baseline, subjects showed an average excess accommodation of 0.50D, possibly due to instrumental factors; up to 1D, average accommodation closely matched the required level; but beyond that, less accommodation than demanded was observed (Atchison & Smith, 2023). This fact was found analyzing the TG but, when only older subjects were studied, they accommodated less under higher demands, as it was expected, due to presbyopia (Anderson et al., 2008). Finally, Table 1 shows a decrease in AA and MAF when the sample is divided into groups, with lower values observed in the older age groups due to presbyopia as expected (Laughton et al., 2017).

An increase in the absolute and relative values of (e, Q, SF) indicated retinal flattening as accommodative demand increased. No studies have evaluated changes in retinal curvature with accommodation across different age ranges. However, similar studies, like Arcas et al. (Arcas-Carbonell et al., 2024), found significant thinning of the parafoveal area (3 mm) with increasing accommodative demand, except in the lower part. This thinning is attributed to the stretching of the non-vascular smooth muscle fibers of the uvea, potentially causing choroidal thinning. This might relate to our findings, suggesting that as the retina flattens, it could also stretch and thin in the central area. In contrast, the perifoveal (6 mm) and peripheral retina (9 mm) showed a tendency towards increased retinal thickness, except in the nasal sector (Arcas-Carbonell et al., 2024).

Studies with MRI have described a less oblate posterior ocular morphology, indicated by lower Q values, correlates with myopic SE and increased AL, as characteristic of myopic eyes. In contrast, non-myopic eyes exhibit a more global expansion, while myopic eyes are predominantly elongated along the axial dimension, resulting in a less oblate form even at early developmental stages. This revealed a consistent association between myopic refraction, increased AL, and a progressively more prolate ocular shape suggesting that, as myopic eyes age and the degree of myopia increases, they maintain a more prolate configuration even when AL decreases (Lim et al., 2020) and, even, variations of this fact can be found by ethnicity (Mohd-Ali et al., 2022; Verkicharla et al., 2017). Focusing on the posterior pole, data from ocular MRIs aged 18 to 36 years (Atchison et al., 2005) showed that most myopes have oblate, rather than prolate, retinal shapes (even up to 12D), varied considerably between subjects with similar refractive errors. In most emmetropic eyes, the shapes were oblate (steepening toward the equator). As myopia increased, the retinal shape became less oblate. However, a few myopic eyes were prolate (flattening toward the equator). Previous studies found dissimilar results on young myopic eyes, with some suggesting distinct accommodative behavior due to their prolate nature (Flitcroft et al., 2019). In our study, when our sample was divided into the five age groups, significant differences were found in the younger groups (G1, G2, and G3), with the retina flattening as the accommodative demand increases, consistent with a prolate behavior. The younger groups also presented a more myopic mean refractive error, which is associated with a more prolate retinal shape (Lim et al., 2020). In older groups, G4 and G5, changes in shape were appreciated without statistical significance, which could be due to presbyopia. Age-related changes, such as lens stiffening, could limit accommodative capacity, and the retina may similarly exhibit reduced adaptability to compensate for high accommodative demands (Bhardwaj & Rajeshbhai, 2013; Ni et al., 2011).

In this study, no statistically significant differences were found in the curvature of the anterior surface of the lens as accommodation was stimulated in the TG. However, there are studies such as that of Dubbelman et al. (Dubbelman & Van Der Heijde, 2001) which corroborate the increase in curvature of the anterior surface of the lens with accommodation, with the change in the radius of curvature in diopters being 4.7 times greater on the anterior surface than on the posterior surface. The increase in curvature of the anterior surface of the lens can be explained with the Helmholtz model, which is because the resting tension of the zonular fibers on the equator of the lens keeps it in a flattened and misaligned state. As the ciliary muscle contracts, the ciliary body moves forward and inward, approaching the equator of the lens. This releases the resting tension of the zonule around the equator. With the relaxation of zonular tension, the lens capsule shapes its contents, reducing its equatorial diameter and increasing its thickness. This allows the anterior and posterior surfaces to increase their curvature, facilitating accommodation (Ishii et al., 2011; Verkicharla et al., 2012). In the case of the study by Xiang et al., it was observed that during accommodation stimulation, the change in lens thickness is primarily due to the lens nucleus, not the cortex. Additionally, the anterior surface of the nucleus advanced forward, while the posterior surface of the nucleus shifted backward, though only slightly (Xiang et al., 2021).

Although no statistically significant differences were found in our study, a certain tendency to increase curvature was observed (Fig. 4A). It was believed that the absence of significant differences was since the area of the lens that was measured was small, since the subjects were undilated and the pupil was around 4–5 mm in diameter on average. It was considered that, if the subjects had been dilated, a larger area of the anterior surface of the lens could have been analyzed and significant differences would surely have been found in the curvature of the lens, increasing its curvature with the accommodative demand, as occurs in Dubbelman et al. (Dubbelman & Van Der Heijde, 2001), in which 5 % phenylephrine HCl was used for pupil dilation, thereby achieving a greater area of the lens to analyze, obtaining significant changes in the curvature of the lens.

In the analysis of the anterior curvature of the lens by age groups, no statistically significant differences were obtained as the accommodative demand increased, observing the tendency for the lens to curve, except in G5, who, being the most presbyopic, cannot carry out the

accommodation required of 5D, and a tendency to relax the accommodation completely was observed (Fig. 4B). In the study mentioned above (Dubbelman & Van Der Heijde, 2001) nor could any dependence of the curvature of the anterior surface of the lens on age be determined. They argued that this correlation had to exist since the change in the curvature of the lens seemed to depend on the shape of the lens when it is not accommodating, thus decreasing the changes produced when the convexity of its surfaces increases. With age, the convexity of the lens increases due to the proliferation of cell layers towards the surface, theoretically decreasing the magnitude of the morphological changes produced (Ruan et al., 2020). Finally, they observed that the change in the curvature of both surfaces of the lens, anterior and posterior, was independent of age and did not depend on the shape of the unaccommodated lens (Dubbelman & Van Der Heijde, 2001). Additionally, another study observed that a younger age and greater anterior curvature of the lens were associated with a higher amplitude of accommodation-induced change in the anterior curvature of the lens (Wang et al., 2022).

Additionally, it was observed that the ACD decreases significantly as the accommodative demand increases in the TG, due to anterior displacement of the lens as it is described in the study by Wang et al. (Wang et al., 2022), where a comparison between eyes in an accommodative state was made, finding that, compared to the non-accommodative state, the ACD tended to decrease in them. As explained by Benozzi et al. (Benozzi et al., 2013), the thickness of the lens increases due to the decrease in its radii of curvature, appearing more curved as it moves forward, which produces a decrease in the ACD as accommodation increases.

When studying the changes in ACD by age groups, a significant decrease was observed as accommodation increases (Fig. 5B), with the most pronounced narrowing in the oldest group, G5 (Fig. 5C). According to Augusteyn et al. (Augusteyn et al., 2011) the sagittal diameter of the lens increases with age due to cortical thickening, causing the lens to move forward while the distance between the corneal vertex and the posterior lens surface remains unchanged. Ni et al. (Ni et al., 2011), observed significant ACD reductions during accommodation in both young and presbyopic groups, although lens curvature changes were only significant in younger individuals. In our study, younger groups (G1, G2 and G3), characterized by deeper ACDs and higher myopia, contrast with older, less myopic groups (G4 and G5), supporting the reported association between refractive error and ACD depth (Bhardwaj & Rajeshbhai, 2013). Although the IOL Master 500 does not measure lens thickness, the narrowing ACD with age is consistent with expected lens thickening. Future research incorporating lens thickness measurements could clarify the interaction between refractive error, lens morphology, and ACD changes across age groups.

By accommodating 3D, the ACD decreases, as do the radii of curvature of the anterior face of the lens, resulting in greater curvature and crystalline power and its anterior displacement. On the other hand, when accommodating 1D, a significant negative correlation was observed between the eccentricity of the anterior surface of the lens and the eccentricity of the retina. That is, as the anterior surface of the lens curves, the retina flattens. These findings indicate that the modifications in the ACD, the curvature of the lens and that of the retina are interrelated and vary according to the degree of accommodative demand, underlining the complexity of the accommodation mechanism and its effects on the ocular structures, both in the anterior pole as well as the posterior pole, being dependent with age.

During the study's development several limitations were identified. Quantitative retinal shape analysis with OCT is known to be challenged by various optical distortions inherent to posterior segment imaging. Although our OCT systems provide enough speed and sensitivity, they could be affected by sensitivity decline and possible artifacts, limiting their axial range. In our study, the goal was not to measure exact absolute values of the transversal structures but to compare a series of measurements with the baseline images. Perhaps these type of limits might be addressed using whole retina images, which appear comparable to MRI measurements (McNabb et al., 2019). Whole-eye imaging, utilizing a single instrument capable of measuring both the anterior and posterior segments, could allow for precise determination of the true retinal shape (Frisken et al., 2023). Our raw data were used to compose the evaluated retinas, but artifacts could be found when peripheral measurements are made, as it happens when refractive error and eye length is measured with commercial devices (Atchison & Rozema, 2023). Furthermore, anterior optics and refractive power changes during accommodation influence the infrared light path, which could affect the distortion of the OCT images and the apparent retinal curvature. Prior studies highlight the importance of correcting these distortions for accurate retinal curvature measurements (Kim et al., 2024; Kuo et al., 2016). Although this study focused on relative, intra-subject changes, supported by a preliminary validation experiment confirming the reliability of uncorrected scans, future research will need to incorporate optical modelling to enhance anatomical accuracy. Lastly, some limitations of the obtained results may be related to the small sample size in certain age groups. The G5 group, in particular, was smaller due to the difficulty in recruiting participants who met the strict inclusion criteria, including no prior ocular pathology, no systemic treatments, and no history of ocular surgery.

5. Conclusion

In conclusion, objective accommodation measurements indicate that subjects adequately respond to low accommodative demands (up to 1D), but their ability diminishes with higher demands, possibly due to presbyopia. Our findings suggest a possible tendency for retinal curvature to flatten as accommodative demand increases; however, given the methodological limitations, this observation requires further validation. Although there is a tendency for the anterior lens surface to become more curved with greater demands, statistical significance was not consistently observed. Additionally, ACD decreases with increasing accommodative demand, with older age groups experiencing greater reductions. These insights underscore the complex interplay between age-related changes in ocular structures and accommodative function. Future studies are necessary to further refine our understanding and potentially enhance clinical approaches in managing presbyopia and other age-related accommodation changes.

Funding sources

This research did not receive any specific grant from funding agencies in the public, commercial, or not-for-profit sectors.

CRediT authorship contribution statement

María Arcas-Carbonell: Writing – original draft, Visualization, Validation, Software, Methodology, Investigation, Formal analysis, Data curation. **Elvira Orduna-Hospital:** Writing – review & editing, Writing – original draft, Visualization, Validation, Supervision, Software, Resources, Project administration, Methodology, Investigation, Formal analysis, Conceptualization. **Sara Oliete-Lorente:** Writing – original draft, Visualization, Validation, Software, Methodology, Investigation, Formal analysis, Data curation. **María Mechó-García:** Writing – original draft, Visualization, Validation, Software, Methodology, Investigation, Formal analysis, Data curation. **Guisela Fernández-Espinosa:** Writing – original draft, Visualization, Validation, Methodology, Investigation, Data curation. **Ana Sanchez-Cano:** Writing – review & editing, Writing – original draft, Visualization, Validation, Supervision, Software, Resources, Project administration, Methodology, Investigation, Formal analysis, Conceptualization.

Declaration of competing interest

The authors declare that they have no known competing financial interests or personal relationships that could have appeared to influence the work reported in this paper.

Appendix A. Supplementary material

Supplementary data to this article can be found online at https://doi.org/10.1016/j.visres.2025.108596.

Data availability

Data will be made available on request.

References

Ahn, S. J., Rauh, W., & Warnecke, H.-J. (2001). Least-squares orthogonal distances fitting of circle, sphere, ellipse, hyperbola, and parabola. *Pattern Recognition, 34*(12), 2283–2303.

Aldaba, M., Vilaseca, M., Díaz-Doutón, F., Arjona, M., & Pujol, J. (2012). Measuring the accommodative response with a double-pass system: Comparison with the Hartmann-Shack technique. *Vision Research, 62*, 26–34.

Anderson, H. A., Stuebing, K. K., Glasser, A., & Manny, R. E. (2008). Influence of accommodative amplitude and age on objective measurements of lag in children and adults. *Investigative Ophthalmology & Visual Science, 49*(13), 4560.

Arcas-Carbonell, M., Orduna-Hospital, E., Fernández-Espinosa, G., Mechó-García, M., Castro-Torres, J. J., & Sánchez-Cano, A. (2024). Anterior chamber and retinal morphological changes during accommodation in different age ranges. *Current Eye Research*, 1–11.

Atchison, D. A., Jones, C. E., Schmid, K. L., Pritchard, N., Pope, J. M., Strugnell, W. E., & Riley, R. A. (2004). Eye shape in emmetropia and myopia. *Investigative Ophthalmology and Visual Science, 45*(10), 3380–3386. https://doi.org/10.1167/iovs.04-0292

Atchison, D. A., Pritchard, N., Schmid, K. L., Scott, D. H., Jones, C. E., & Pope, J. M. (2005). Shape of the retinal surface in emmetropia and myopia. *Investigative Ophthalmology and Visual Science, 46*(8), 2698–2707. https://doi.org/10.1167/iovs.04-1506

Atchison, D. A., & Rozema, J. J. (2023). Technical notes on peripheral refraction, peripheral eye length and retinal shape determination. *Ophthalmic and Physiological Optics, 43*(3), 584–594. https://doi.org/10.1111/opo.13097

Atchison, D. A., & Smith, G. (2023). Optics of the Human Eye: Second Edition. *Optics of the Human Eye: Second Edition*, 1–478. https://doi.org/10.1201/9781003128601/OPTICS-HUMAN-EYE-DAVID-ATCHISON

Augusteyn, R. C., Mohamed, A., Nankivil, D., Veerendranath, P., Arrieta, E., Taneja, M., … Parel, J. M. (2011). Age-dependence of the optomechanical responses of ex vivo human lenses from India and the USA, and the force required to produce these in a lens stretcher: the similarity to in vivo disaccommodation. *Vision research, 51*(14), 1667–1678.

Beenakker, J.-W.-M., Shamonin, D. P., Webb, A. G., Luyten, G. P. M., & Stoel, B. C. (2015). Automated retinal topographic maps measured with magnetic resonance imaging. *Investigative Ophthalmology and Visual Science, 56*(2), 1033–1039. https://doi.org/10.1167/iovs.14-15161

Benozzi, G., Leiro, J., Facal, S., Perez, C., Benozzi, J., & Orman, B. (2013). Developmental changes in accommodation evidenced by an ultrabiomicroscopy procedure in patients of different ages. *Medical Hypothesis, Discovery & Innovation Ophthalmology Journal, 2*(1), 8–13.

Bhardwaj, V., & Rajeshbhai, G. P. (2013). Axial length, anterior chamber depth-a study in different age groups and refractive errors. *Journal of Clinical and Diagnostic Research: JCDR, 7*(10), 2211.

Calossi, A. (2007). Corneal asphericity and spherical aberration. *Journal of Refractive Surgery, 23*(5), 505–514.

Cheng, H. M., Singh, O. S., Kwong, K. K., Xiong, J., Woods, B. T., & Brady, T. J. (1992). Shape of the myopic eye as seen with high-resolution magnetic resonance imaging. *Optometry and Vision Science, 69*(9), 698–701. https://doi.org/10.1097/00006324-199209000-00005

Downs, J. W. (2003). *Practical conic sections: The geometric properties of ellipses, parabolas and hyperbolas. Courier Corporation.*

Dubbelman, M., & Van Der Heijde, G. L. (2001). The shape of the aging human lens: Curvature, equivalent refractive index and the lens paradox. *Vision Research, 41*(14), 1867–1877. https://doi.org/10.1016/S0042-6989(01)00057-8

Fan, R., Chan, T. C. Y., Prakash, G., & Jhanji, V. (2018). Applications of corneal topography and tomography: A review. *Clinical & Experimental Ophthalmology, 46*(2), 133–146.

Fan, S., Sun, Y., Dai, C., Zheng, H., Ren, Q., Jiao, S., & Zhou, C. (2014). Accommodation-induced variations in retinal thickness measured by spectral domain optical coherence tomography. *Journal of Biomedical Optics, 19*(9). https://doi.org/10.1117/1.JBO.19.9.096012

Faria-Ribeiro, M., López-Gil, N., Navarro, R., Lopes-Ferreira, D., Jorge, J., & González-Méijome, J. M. (2014). Computing retinal contour from optical biometry. *Optometry and Vision Science, 91*(4), 430–436. https://doi.org/10.1097/OPX.0000000000000225

Flitcroft, D. I., He, M., Jonas, J. B., Jong, M., Naidoo, K., Ohno-Matsui, K., Rahi, J., Resnikoff, S., Vitale, S., & Yannuzzi, L. (2019). IMI - defining and classifying myopia: A proposed set of standards for clinical and epidemiologic studies. *Investigative Ophthalmology & Visual Science, 60*(3), M20–M30. https://doi.org/10.1167/iovs.18-25957

Frisken, S., Anderson, T., Segref, A., Lorenser, D., & Frisken, G. (2023). Anterior and posterior imaging with hyperparallel OCT. *Biomedical Optics Express, 14*(6), 2678–2688. https://doi.org/10.1364/BOE.488810

Giovanzana, S., Evans, T., & Pierscionek, B. (2017). Lens internal curvature effects on age-related eye model and lens paradox. *Biomedical Optics Express, 8*(11), 4827–4837.

Ishii, K., Iwata, H., & Oshika, T. (2011). Quantitative evaluation of changes in eyeball shape in emmetropization and myopic changes based on elliptic Fourier descriptors. *Investigative Ophthalmology and Visual Science, 52*(12), 8585–8591. https://doi.org/10.1167/iovs.11-7221

Kanellopoulos, A. J., & Asimellis, G. (2014). Clear-cornea cataract surgery: Pupil size and shape changes, along with anterior chamber volume and depth changes. *A Scheimpflug imaging study. Clinical Ophthalmology*, 2141–2150.

Kanski, J. J., & Bowling, B. (2011). *Clinical ophthalmology: A systematic approach*. Elsevier Health Sciences.

Kim, Y. W., Sharpe, G. P., Siber, J., Keßler, R., Fischer, J., Otto, T., & Chauhan, B. C. (2024). Critical impact of working distance on OCT imaging: correction of optical distortion and its effects on measuring retinal curvature. *Investigative Ophthalmology & Visual Science, 65*(12), 10.

Koretz, J. F., Cook, C. A., & Kaufman, P. L. (2001). Aging of the human lens: Changes in lens shape at zero-diopter accommodation. *JOSA A, 18*(2), 265–272.

Koretz, J. F., Cook, C. A., & Kaufman, P. L. (2002). Aging of the human lens: Changes in lens shape upon accommodation and with accommodative loss. *Journal of the Optical Society of America. A, Optics, Image Science, and Vision, 19*(1), 144–151. https://doi.org/10.1364/josaa.19.000144

Koumbo Mekountchou, I. O., Conrad, F., Sankaridurg, P., & Ehrmann, K. (2020). Peripheral eye length measurement techniques: A review. *Clinical and Experimental Optometry, 103*(2), 138–147. https://doi.org/10.1111/cxo.12892

Kuo, A. N., Verkicharla, P. K., McNabb, R. P., Cheung, C. Y., Hilal, S., Farsiu, S., Chen, C., Wong, T. Y., Ikram, M. K., & Cheng, C. Y. (2016). Posterior eye shape measurement with retinal OCT compared to MRI. *Investigative Ophthalmology & Visual Science, 57*(9), Article OCT196–OCT203.

Laughton, D. S., Sheppard, A. L., Mallen, E. A. H., Read, S. A., & Davies, L. N. (2017). Does transient increase in axial length during accommodation attenuate with age? *Clinical and Experimental Optometry, 100*(6), 676–682.

Li, Q., & Fang, F. (2021). Retinal contour modelling to reproduce two-dimensional peripheral spherical equivalent refraction. *Biomedical Optics Express, 12*(7), 3948. https://doi.org/10.1364/boe.426413

Lim, L. S., Matsumura, S., Htoon, H. M., Tian, J., Lim, S. B., Sensaki, S., Chen, C., Hilal, S., Wong, T. Y., Cheng, C. Y., Kuo, A., & Saw, S. M. (2020). MRI of posterior eye shape and its associations with myopia and ethnicity. *British Journal of Ophthalmology, 104*(9), 1239–1245. https://doi.org/10.1136/bjophthalmol-2019-315020

McNabb, R. P., Polans, J., Keller, B., Jackson-Atogi, M., James, C. L., Vann, R. R., Izatt, J. A., & Kuo, A. N. (2019). Wide-field whole eye OCT system with demonstration of quantitative retinal curvature estimation. *Biomedical Optics Express, 10*(1), 338–355. https://doi.org/10.1364/BOE.10.000338

Mejía-Barbosa, Y., & Malacara-Hernández, D. (2001). A review of methods for measuring corneal topography. *Optometry and Vision Science: Official Publication of the American Academy of Optometry, 78*(4), 240–253. https://doi.org/10.1097/00006324-200104000-00013

Mohd-Ali, B., Chen, L. Y., Shahimin, M. M., Arif, N., Hamid, H. A., Halim, W. H. W. A., Mokri, S. S., Huddin, A. B., & Mohidin, N. (2022). Ocular dimensions by three-dimensional magnetic resonance imaging in emmetropic versus myopic school children. *Medical Hypothesis, Discovery, and Innovation in Ophthalmology, 11*(2), 64–70. https://doi.org/10.51329/mehdiophthal1447

Ni, Y., Liu, X.-L., Wu, M.-X., Lin, Y., Sun, Y.-Y., He, C., & Liu, Y.-Z. (2011). Objective evaluation of the changes in the crystalline lens during accommodation in young and presbyopic populations using Pentacam HR system. *International Journal of Ophthalmology, 4*(6), 611.

Orduna-Hospital, E., Ávila, F. J., Fernández-Espinosa, G., & Sanchez-Cano, A. (2022). Lighting-induced changes in central and peripheral retinal thickness and shape after short-term reading tasks in electronic devices. *Photonics, 9*(12). https://doi.org/10.3390/photonics9120990

Orduna-Hospital, E., Sanchez-Bautista, J. J., Fernández-Espinosa, G., Arcas-Carbonell, M., & Sanchez-Cano, A. (2024). Optical and retinal changes influenced by different lighting conditions. *Experimental Eye Research, 110146*.

Pope, J. M., Verkicharla, P. K., Sepehrband, F., Suheimat, M., Schmid, K. L., & Atchison, D. A. (2017). Three-dimensional MRI study of the relationship between eye dimensions, retinal shape and myopia. *Biomedical Optics Express, 8*(5), 2386–2395. https://doi.org/10.1364/BOE.8.002386

Ruan, X., Liu, Z., Luo, L., & Liu, Y. (2020). Structure of the lens and its associations with the visual quality. *BMJ Open Ophthalmology, 5*(1), Article e000459.

Rutter, J. W. (2018). *Geometry of curves*. Chapman and Hall/CRC.

Verkicharla, P. K., Mathur, A., Mallen, E. A. H., Pope, J. M., & Atchison, D. A. (2012). Eye shape and retinal shape, and their relation to peripheral refraction. *Ophthalmic and Physiological Optics, 32*(3), 184–199. https://doi.org/10.1111/j.1475-1313.2012.00906.x

Verkicharla, P. K., Suheimat, M., Schmid, K. L., & Atchison, D. A. (2016). Peripheral refraction, peripheral eye length, and retinal shape in Myopia. *Optometry and Vision Science, 93*(9), 1072–1078. https://doi.org/10.1097/OPX.0000000000000905

Verkicharla, P. K., Suheimat, M., Schmid, K. L., & Atchison, D. A. (2017). Differences in retinal shape between East Asian and Caucasian eyes. *Ophthalmic and Physiological Optics, 37*(3), 275–283. https://doi.org/10.1111/opo.12359

Wang, L., Jin, G., Ruan, X., Gu, X., Chen, X., Wang, W., Dai, Y., Liu, Z., & Luo, L. (2022). Changes in crystalline lens parameters during accommodation evaluated using swept source anterior segment optical coherence tomography. *Annals of Eye Science, 7*(1), 33.

Wang, Y., Shao, Y., & Yuan, Y. (2015). Simultaneously measuring ocular aberration and anterior segment biometry during accommodation. *Journal of Innovative Optical Health Sciences, 8*(02), Article 1550005.

Wolffsohn, J. S., & Davies, L. N. (2019). Presbyopia: Effectiveness of correction strategies. *Progress in Retinal and Eye Research, 68*, 124–143.

Xiang, Y., Fu, T., Xu, Q., Chen, W., Chen, Z., Guo, J., Deng, C., Manyande, A., Wang, P., & Zhang, H. (2021). Quantitative analysis of internal components of the human crystalline lens during accommodation in adults. *Scientific Reports, 11*(1), 6688.

Ying, J., Wang, B., & Shi, M. (2012). Anterior corneal asphericity calculated by the tangential radius of curvature. *Journal of Biomedical Optics, 17*(7), 75005.